the FEBS Journal

Identification of two p23 co-chaperone isoforms in *Leishmania braziliensis* exhibiting similar structures and Hsp90 interaction properties despite divergent stabilities

Fernanda A.H. Batista[1*], Glessler S. Almeida[2*], Thiago V. Seraphim[1], Kelly P. Silva[1], Silvane M.F. Murta[3], Leandro R.S. Barbosa[4] and Júlio C. Borges[1]

1 Instituto de Química de São Carlos, Universidade de São Paulo - USP, São Carlos, SP, Brazil
2 Programa de Pós-Graduação em Genética Evolutiva e Biologia Molecular, Departamento de Genética e Evolução, Universidade Federal de São Carlos, São Carlos, SP, Brazil
3 Centro de Pesquisa René Rachou, Fiocruz, Belo Horizonte, MG, Brazil
4 Instituto de Física, Universidade de São Paulo - USP, São Paulo, SP, Brazil

Keywords
Hsp90; *L. braziliensis*; molecular chaperones; p23; protozoa

Correspondence
J. C. Borges, Instituto de Química de São Carlos, Universidade de São Paulo – USP, PO Box 780, São Carlos 13560-970, SP, Brazil
Fax: +55 16 3373 9982
Tel: +55 16 3373 8637
E-mail: borgesjc@iqsc.usp.br

*These authors contributed equally to this work

(Received 8 August 2014, revised 28 October 2014, accepted 31 October 2014)

doi:10.1111/febs.13141

The small acidic protein called p23 acts as a co-chaperone for heat-shock protein of 90 kDa (Hsp90) during its ATPase cycle. p23 proteins inhibit Hsp90 ATPase activity and show intrinsic chaperone activity. A search for p23 in protozoa, especially trypanosomatids, led us to identify two putative proteins in the *Leishmania braziliensis* genome that share approximately 30% identity with each other and with the human p23. To understand the presence of two p23 isoforms in trypanosomatids, we obtained the recombinant p23 proteins of *L. braziliensis* (named Lbp23A and Lbp23B) and performed structural and functional studies. The recombinant proteins share similar solution structures; however, temperature- and chemical-induced unfolding experiments showed that Lbp23A is more stable than Lbp23B, suggesting that they may have different functions. Lbp23B prevented the temperature-induced aggregation of malic dehydrogenase more efficiently than did Lbp23A, whereas the two proteins had equivalent efficiencies with respect to preventing the temperature-induced aggregation of luciferase. Both proteins interacted with *L. braziliensis* Hsp90 (LbHsp90) and inhibited its ATPase activity, although their efficiencies differed. *In vivo* identification studies suggested that both proteins are present in *L. braziliensis* cells grown under different conditions, although Lbp23B may undergo post-translation modifications. Interaction studies indicated that both Lbp23 proteins interact with LbHsp90. Taken together, our data suggest that the two protozoa p23 isoforms act similarly when regulating Hsp90 function. However, they also have some differences, indicating that the *L. braziliensis* Hsp90 machine has features providing an opportunity for novel forms of selective inhibition of protozoan Hsp90.

Introduction

Heat-shock protein of 90 kDa (Hsp90) is an important molecular chaperone that stabilizes client proteins in a competent state to trap intracellular signals using a dynamic interaction cycle [1,2]. To function properly,

Abbreviations
aSEC, analytical size exclusion chromatography; *D*, diffusion coefficient; DSC, differential scanning calorimetry; hp23, human p23; Hsp90, heat-shock protein of 90 kDa; ITC, isothermal titration calorimetry; MDH, malic dehydrogenase; MM, molecular mass; SAXS, small-angle X-ray scattering; SE-AUC, sedimentation equilibrium-analytical ultracentrifugation; SV-AUC, sedimentation velocity-analytical ultracentrifugation.

the Hsp90 machinery is assisted by a wide range of co-chaperones regulating the Hsp90 functional cycle and dictating the fate of Hsp90, as well as the protein client [2–4].

The small acidic protein p23 is a co-chaperone that recognizes ATP-bound Hsp90 [5–7] and stimulates Hsp90-substrate dissociation [7,8]. Human p23 (hp23) possesses an N-terminal core that folds into a β-sheet structure and an unstructured C-terminal tail [8,9]. The p23–Hsp90 interaction occurs via an extensive surface area of the β-sheet core domain of p23, which appears to be sufficient for the interaction [9–11]. In yeast, the interaction between p23 (Sba1) and Hsp90 (yHsp90) leads to dimerization of the Hsp90 N-terminal domain [12,13]. This finding was confirmed in the crystal structure of the Sba1–Hsp90 complex, which revealed that one Sba1 molecule interacts with two dimerized N-terminal and middle domains of the Hsp90 dimer in a 2 : 1 stoichiometry [14]. Human p23 interacts with Hsp90 either in the presence or absence of ATP [15] via contacts with the Hsp90 N-terminal and middle domains [11,15,16]. The interaction between hp23 and Hsp90 involves the lid of the ATP-binding site at the N-terminal domain and modulates the environment of the ATP pocket, leading to a non-hydrolyzable state; the interaction also induces changes in the Hsp90 middle domain [17].

The importance of p23 for the Hsp90 action cycle has been demonstrated using the Hsp90 inhibitors geldanamycin and radicicol, which prevent the proper interaction between Hsp90 and p23, thus stopping the Hsp90 functional cycle [18] and leading substrates to degradation machinery [12,19]. The absence of p23 in yeast and mammalian cells leads to hypersensitivity to those Hsp90 inhibitors [10]. *In vitro*, p23 also presents intrinsic chaperone activity by holding partially unfolded proteins in a competent state for folding [20,21], amongst other activities [22].

The parasitic disease leishmaniasis is caused by protozoa of the genus *Leishmania*. It is one of the so-called 'neglected diseases' that mainly affects people in low-income regions [23,24] and remains an important health-care challenge, including the need to develop new drugs for more effective treatments [4,25]. In this context, molecular chaperones have been indicated as a target for the development of drugs against protozoa [26–29] because they are essential for protein metabolism [1,4]. The search for p23 in protozoa led us to identify two putative protein candidates in the *Leishmania braziliensis* genome, as well as in other trypanosomatids; these proteins share approximately 30% identity with each other and with hp23. To explain the presence of two p23 proteins in trypanosomatids, we obtained the recombinant p23s of *L. braziliensis* (Lbp23A and Lbp23B) and investigated their structure and function. We show that these proteins have differences in stability, despite similarities in their protein structures; they also have different intrinsic chaperone activities. Both proteins inhibit LbHsp90 ATPase activity but with different efficiencies, and they are present in *L. braziliensis* cells. Interaction studies demonstrated that both Lbp23 proteins interact with LbHsp90 dimer in a 1 : 1 stoichiometry and similar K_D values in the presence and absence of adenosine nucleotides.

Results

Sequence analysis, expression and purification

Figure 1A shows the amino acid sequences of Lbp23A and Lbp23B, which were aligned to the amino acid sequence of hp23. The Lbp23 proteins show 21% identity in their amino acid sequences. Compared with hp23, Lbp23A and Lbp23B show 33% and 23% identity, respectively (Fig. 1A). Despite this low identity, Lbp23 shows a high conservation degree with hp23 considering the Trp residues, as well as the WPRLTKE sequence, which is described as a signature motif of p23 proteins [9]. Martinez-Yamout *et al.* [11] identified several residues in hp23 that are involved in the interaction with human Hsp90. A close inspection of these residues in the Lbp23 sequences showed a high degree of conservation with little (D10, R12, Y14, F16, E81, G83, R93, L96, S100, V101, K107, W109, E110, D111 and D112) or no (W8, R11, V15, W86, R88, W106 and D108) differences in the residue positions (the residues are numbered according to the hp23 sequence) (Fig. 1A), indicating that both Lbp23 proteins may interact with Hsp90 via a similar surface.

Using the hp23 sequence as a query, we performed a BLAST search on the GenBank database (http://www.ncbi.nlm.nih.gov) for the p23 protein of organisms belonging to the Plasmodiidae and Trypanosomatidae families. Similar to *L. braziliensis*, nine other organisms presented two p23 sequences. Using the sequence of the hp23 crystallographic structure [9] and the surface interaction of hp23 with Hsp90 [11], we performed an alignment of the conserved region and obtained a dendrogram (Fig. 1B), which shows a clustering of these proteins into two main groups, named 'A' and 'B'. Interestingly, the 'A' group shares highest sequence identity with hp23, whereas the 'B' group has the highest identity with Sba1 (Fig. 1B). We performed an alignment of the p23 sequences, including the

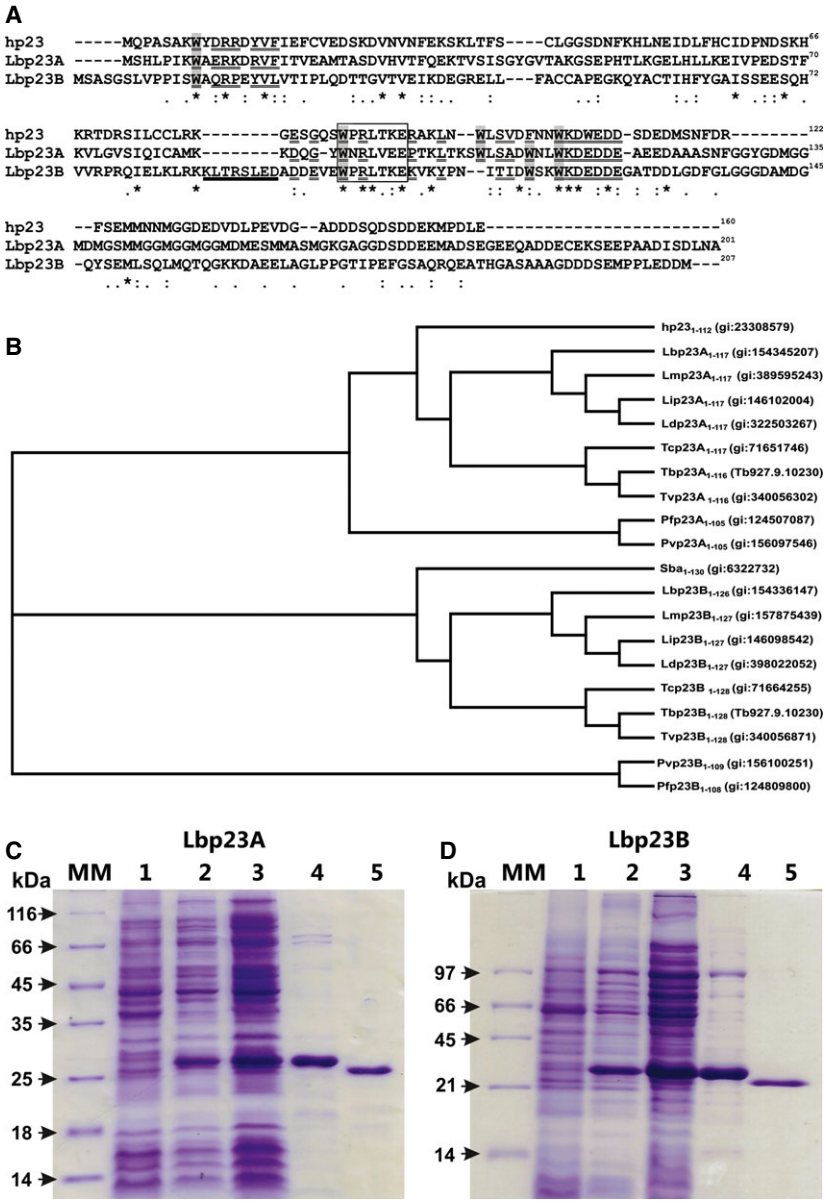

Fig. 1. Sequence analysis and production of Lbp23 proteins. (A) Amino acid sequence alignment among hp23, Lbp23A and Lbp23B, showing the p23 signature motif (in the square), the conserved Trp (in gray) and the residues related to the interaction with Hsp90 (underlined amino acids), in accordance with a previous study [11]. The Lbp23 proteins share 21% identity in their amino acid sequences. The hp23 protein shares 33% and 23% identity with Lbp23A and Lbp23B, respectively. It is worth noting that a sequence of eight amino acids (underlined) is inserted into Lbp23B just before the p23 signature motif. The inserted sequence is also observed for other Trypanosomatids p23B proteins (data not shown). (B) Dendrogram for the multiple-sequence analysis of the p23 protein from *Homo sapiens* (hp23), *Saccharomyces cerevisiae* (Sba1), two species of the Plasmodiidae family and seven species of the Trypanosomatidae family. The alignment was performed based on the sequence of the p23 region from hp23 and considering the amino acids involved in the interaction with human Hsp90 [11]. Organism names used in the alignment: h, *H. sapiens*; Sba, *S. cerevisiae* S288c; Lb, *L. braziliensis* MHOM/BR/75/M2904; Li, *Leishmania infantum* JPCM5; Lm, *Leishmania major* strain Friedlin; Ld, *Leishmania donovani* BPK282A1; Tb, *Trypanosoma brucei* TREU927; Tc, *Trypanosoma cruzi* strain CL Brener; Tv, *Trypanosoma vivax* Y486; Pf, *Plasmodium falciparum* 3D7; and Pv, *Plasmodium vivax* Sal-1. The subscript numbers correspond to the residues used to perform the alignment. The GenBank access code for each protein is indicated in parentheses. The alignment and the tree construction were performed using CLUSTALW2. (C, D) 12% SDS/PAGE showing the expression and purification of Lbp23A and Lbp23B, respectively. MM, protein ladder; 1, non-induced cells; 2, induced cells; 3, supernatant of lysed cells; 4, protein purified by Ni^{2+}-affinity chromatography; 5, protein after the His-tag cleavage with thrombin and after purification by SEC. Both Lbp23 proteins were obtained in the soluble state at more than 95% purity.

sequences of hp23 and Sba1 (data not shown), and observed that the Trypanosomatidae 'B' group has a conserved insertion just before the WPRLTKE sequence motif (Fig. 1A). The inserted sequence may be a signature motif for this group of proteins.

To study the structure–function relationship of Lbp23A and Lbp23B and to help to determine the reason for the existence of two p23 isoforms in the *L. braziliensis* genome, we produced these recombinant proteins (see Materials and methods). Both proteins were well expressed in the soluble fraction of lysed cells (Fig. 1C,D, lane 3) and were purified by affinity chromatography (Fig. 1C,D, lane 4). For biophysical and structural experiments, the N-terminal His-tag was cleaved by thrombin, and the proteins were further purified by size exclusion chromatography (Fig. 1C,D, lane 5). Both Lbp23 proteins were obtained with more than 95% purity.

Both p23 recombinant proteins were produced in the folded state

The secondary structure content of Lbp23A and Lbp23B was assessed by CD spectropolarimetry (Fig. 2A). The measured CD spectra show a similar shape for both proteins where negative bands at around 215–218 nm of different intensities can be observed, which indicates that both proteins have a β-sheet secondary structure content, as demonstrated for hp23 [8,11]. Despite the similarities, Lbp23A showed a higher residue molar ellipticity ([θ]) signal at approximately 200 nm and a smaller [θ] signal at 218 nm than Lbp23B, suggesting that the latter protein may have a higher amount of secondary structure than the first.

Both proteins have a positive band at approximately 230 nm with different intensities (Fig. 2A), which is also characteristic of hp23 [8,11]. This CD signal has been related to aromatic amino acids and possibly influences the secondary structure signal [30].

As shown in Fig. 1A, Lbp23A has five Trp residues, whereas Lbp23B has four residues. This allowed for monitoring of the tertiary structure around the residues (named here as the local tertiary structure) of both Lbp23 proteins using intrinsic fluorescence emission. The recorded values of λ_{max} were 341 ± 1 nm and 342 ± 1 nm for Lbp23A and Lbp23B, respectively. The calculated spectral center of mass (<λ>) values for Lbp23A and Lbp23B were 352.0 ± 0.4 nm and 351.2 ± 0.3 nm, respectively. The fluorescence emission properties of the tryptophan change depending on this exposure to a nonpolar–polar environment. Buried or partially buried tryptophan residues display an λ_{max} < 335 nm, a partially exposed one shows an λ_{max} in the range 340–350 nm, whereas a completely exposed tryptophan displays an λ_{max} of 355 nm [31]. These differences allow monitoring changes in the folded state of a protein upon unfolding. Processes that lead to a protein unfolding, and a consequent tertiary structure disclosure, induce a solvent tryptophan exposure with resulting changes in the fluorescent emission parameters [31]. In this way, a direct inspection of the fluorescence emission spectra (Fig. 2B) suggested that both proteins have local tertiary structure, once Trp exhibits λ_{max} values that are compatible to partially exposed residues.

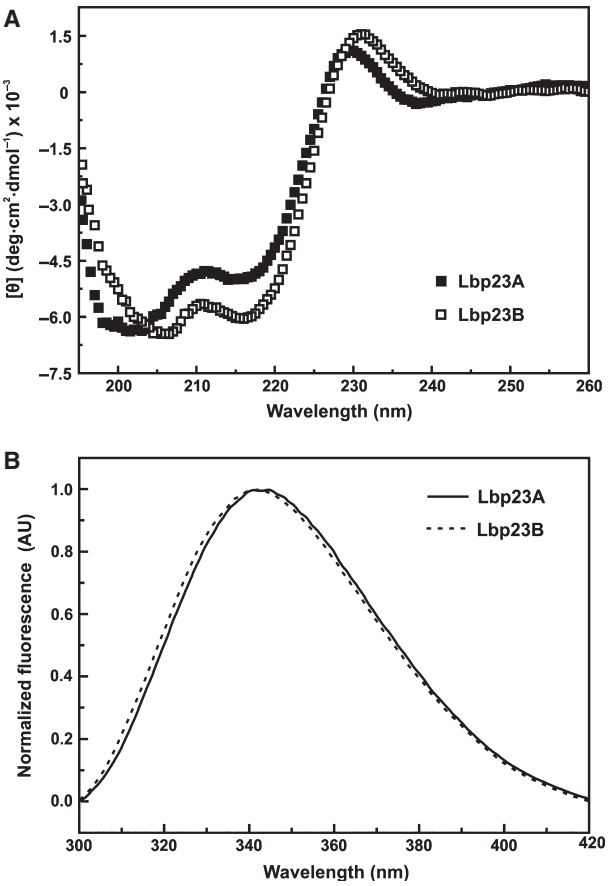

Fig. 2. Spectroscopic characterization of Lbp23A and Lbp23B. (A) CD experiments were performed with Lbp23A and Lbp23B and indicated that the two proteins have similar secondary structure content. Both proteins showed negative bands at approximately 215–218 nm of different intensities, which indicates that both proteins have a β-sheet secondary structure content. Lbp23A and Lbp23B also presented a positive band at approximately 230 nm, which is also observed for hp23. (B) Fluorescence experiments were performed using Lbp23A and Lbp23B in the same buffer as for the CD experiments.

Altogether, the spectroscopic characterization suggested that the produced recombinant proteins were folded and share features with other p23 proteins.

Hydrodynamic results show that the Lbp23 proteins are elongated monomers in solution

To obtain more information about the structure of both Lbp23 proteins, analytical size exclusion chromatography (aSEC) experiments were performed, where both proteins eluted between the 45–67 kDa globular protein markers (Fig. 3A). The Stokes radius (R_S) values measured by aSEC were 33 ± 1 Å and 32 ± 1 Å for Lbp23A and Lbp23B, respectively (Table 1). Using the theoretical R_S for a spherical particle with the same molecular mass (MM) allowed a calculation of the frictional ratio (f/f_0) for Lbp23A and Lbp23B, which was 1.5 ± 0.1 and 1.4 ± 0.1, respectively (Table 1). These results indicate that both Lbp23 proteins may be dimers or have an elongated shape.

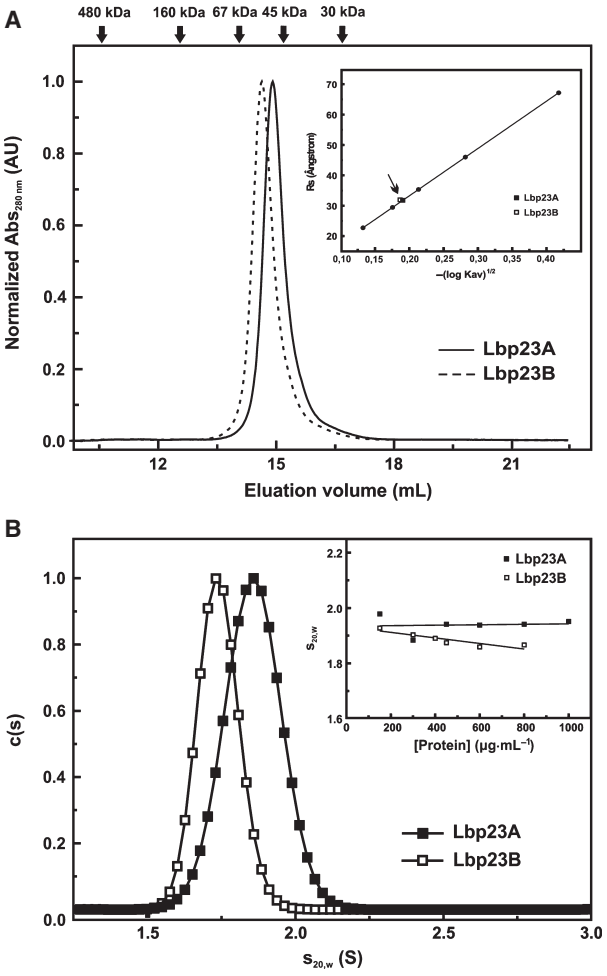

Fig. 3. Hydrodynamic properties of Lbp23A and Lbp23B. (A) The aSEC elution profile showed that Lbp23A and Lbp23B eluted between standard proteins that had molecular masses of 45 and 67 kDa. Inset: estimation of the R_S of Lbp23A and Lbp23B. (B) SV-AUC experiments were performed using various concentrations of Lbp23A and Lbp23B (100 to 800 µg·mL^{-1}). The c(S) distribution curves revealed that both Lbp23 proteins behaved as homogeneous solutions with an $s^0_{20,w}$ of approximately 1.9 *s* for both proteins (inset). The hydrodynamic data are summarized in Table 1.

To further investigate the Lbp23 structure in solution, sedimentation velocity-analytical ultracentrifugation (SV-AUC) experiments were performed. Figure 3B shows the *c*(*S*) distribution function for Lbp23A and Lbp23B at 800 µg·mL^{-1}, suggesting that they behaved as a monodisperse system. The MM values estimated by SEDFIT for Lbp23A and Lbp23B were 23 ± 1 kDa and 26 ± 1 kDa, respectively, indicating that they are monomers in solution. The $s_0$20,w values obtained as a function of protein concentration (Fig. 3B, inset) were 1.94 ± 0.02 s for Lbp23A and 1.89 ± 0.01 s for Lbp23B (Table 1). The f/f_0 values estimated for Lbp23A and Lbp23B from the SV-AUC experiments were 1.46 ± 0.01 and 1.65 ± 0.02, respectively. These results indicated that both Lbp23 proteins have an elongated shape, as observed for hp23 [15] (data not shown). Taken together, all of the hydrodynamic data suggest that both Lbp23A and Lbp23B behave as elongated monomers in solution.

Small-angle X-ray scattering (SAXS) experiments confirm that the Lbp23 proteins are structurally similar and have an elongated shape

To further investigate the structural features of the proteins Lbp23A and Lbp23B, SAXS were performed. Figure 4A shows the scattering curves for Lbp23A and Lbp23B, which were similar. Analysis of the Guinier region of the scattering curves (data not shown) revealed that the Lbp23 proteins behaved as a monodisperse system, with radius of gyration (R_g) values of 33.1 ± 0.5 Å for Lbp23A and 30.1 ± 0.5 Å for Lbp23B. The pair distance distribution functions, *p*(*r*), were generated and exhibited a maximum dimension (D_{max}) of 130 ± 5 Å for both proteins (Fig. 4B), indicating that both Lbp23 proteins have an elongated shape. Consistent with the structural resemblance of the two proteins, the Kratky plot (Fig. 4B, insets) showed that Lbp23A and Lbp23B possess a similar structural compactness and folded core. The *ab initio* models of Lbp23A and Lbp23B (Fig. 4C) highlight the similar overall structural features of these two proteins, and HYDROPRO analysis of both models revealed a good agreement between the R_S, R_g and D_{max} properties and the experimental values (Table 1). The $s_{20,w}$ values were slightly different from the experimental data because HYDROPRO calculates the hydrodynamic properties from the static *ab initio* model and does not consider the protein flexibility in solution [32].

Table 1. Summary of Lbp23A and Lbp23B structural features.

Technique	Property	Protein	
		Lbp23A	Lbp23B
Predicted hydrodynamic data	MM_{pred} (kDa)[a]	22.090	23.045
	R_0 (Å)[a]	18	19
Analytical SEC	R_S (Å)	33 ± 1	32 ± 1
	f/f_0[b]	1.5 ± 0.1	1.4 ± 0.1
AUC	$s^0_{20,w}$ (S)	1.94 ± 0.02	1.89 ± 0.01
	MM_{exp} (kDa)	23 ± 1	26 ± 1
	f/f_0[c]	1.46 ± 0.01	1.65 ± 0.02
SAXS	R_g (Å)	33.1 ± 0.5	30.1 ± 0.5
	D_{max} (Å)	130 ± 5	130 ± 5
HYDROPRO[d]	R_S (Å)	34	34
	R_g (Å)	34	32
	D_{max} (Å)	127	121
	$s_{20,w}$	1.55	1.64

[a] Values predicted for Lbp23A and Lbp23B as a globular monomers in water and 20 °C (predicted by SEDNTERP).
[b] From the ratio of R_S by R_0.
[c] Obtained from SedFit analysis.
[d] Data obtained by the HYDROPRO analysis of the final *ab initio* models.

In summary, these results suggest that Lbp23A and Lbp23B are elongated proteins with a prolate shape in solution. Furthermore, both proteins are very structurally similar in terms of dimension, flexibility and global shape.

Lbp23 proteins have divergent protein stabilities

The structural stability of Lbp23A and Lbp23B was investigated comparatively using thermal- and chemical-induced unfolding experiments, although these unfolding experiments were irreversible for the tested conditions (data not shown).

Because the Lbp23A and Lbp23B proteins both have a positive band at approximately 230 nm, we monitored the thermal-induced unfolding using CD at 231 nm. Figure 5A shows the Lbp23A and Lbp23B thermal-induced unfolding, where both proteins presented a cooperative transition with a T_m at 53.0 ± 0.5 °C and 44.0 ± 0.5 °C for Lbp23A and Lbp23B, respectively (Table 2). We also studied the thermal stability of the Lbp23 proteins using differential scanning calorimetry (DSC) (Fig. 5B), where Lbp23A showed a thermal transition centered at 53.9 ± 0.2 °C, whereas Lbp23B transitioned at 45.1 ± 0.1 °C (Table 2). The calculated ΔH^{cal}_{app} for both Lbp23 proteins was approximately 115 kcal·mol^{-1}.

We monitored the chemical stability of both Lbp23 proteins by following the intrinsic fluorescence

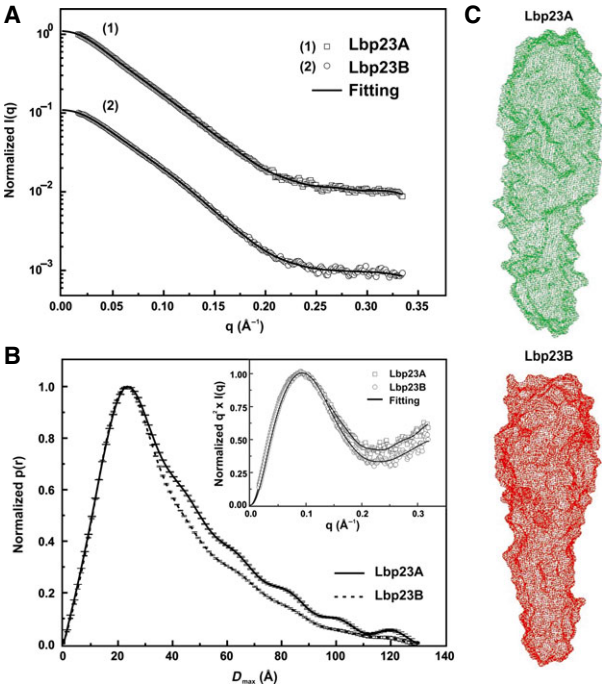

Fig. 4. SAXS studies of the Lbp23 proteins. (A) SAXS curves of Lbp23A and Lbp23B (scaled one order of magnitude for comparison). The solid lines for both proteins (A) represent the curve fitting by GNOM. (B) Particle distance distribution function [$p(r)$ functions] of Lbp23A and Lbp23B. The D_{max} values for both proteins was 130 ± 5 Å, and the $p(r)$ functions were consistent with those for prolate-shaped proteins. Inset: The Kratky plot of Lbp23A and Lbp23B revealed that the two proteins demonstrate similar flexibility. (C) *Ab initio* envelopes of Lbp23A and Lbp23B.

emission signal represented by the <λ> signal (Fig. 5C). In these experiments, we also observed that Lbp23A has higher chemical stability than Lbp23B based on the calculated C_m: the C_m(urea) of Lbp23A was 0.6 M lower than that of Lbp23B (Table 2). Altogether, both the thermal- and chemical-induced unfolding experiments showed that Lbp23A is more stable than Lbp23B.

Lbp23 proteins have different intrinsic chaperone activity

The ability of Lbp23 to prevent temperature-induced protein aggregation was tested comparatively using two model client proteins: malic dehydrogenase (MDH) and luciferase (Fig. 6). These two proteins have been used as hp23 model client proteins [8,9]. Our results indicated that both Lbp23 proteins prevented the thermal aggregation of MDH; however, Lbp23B was more efficient than Lbp23A. The latter appears to co-aggregate with MDH at a low molar ratio, whereas Lbp23B prevented

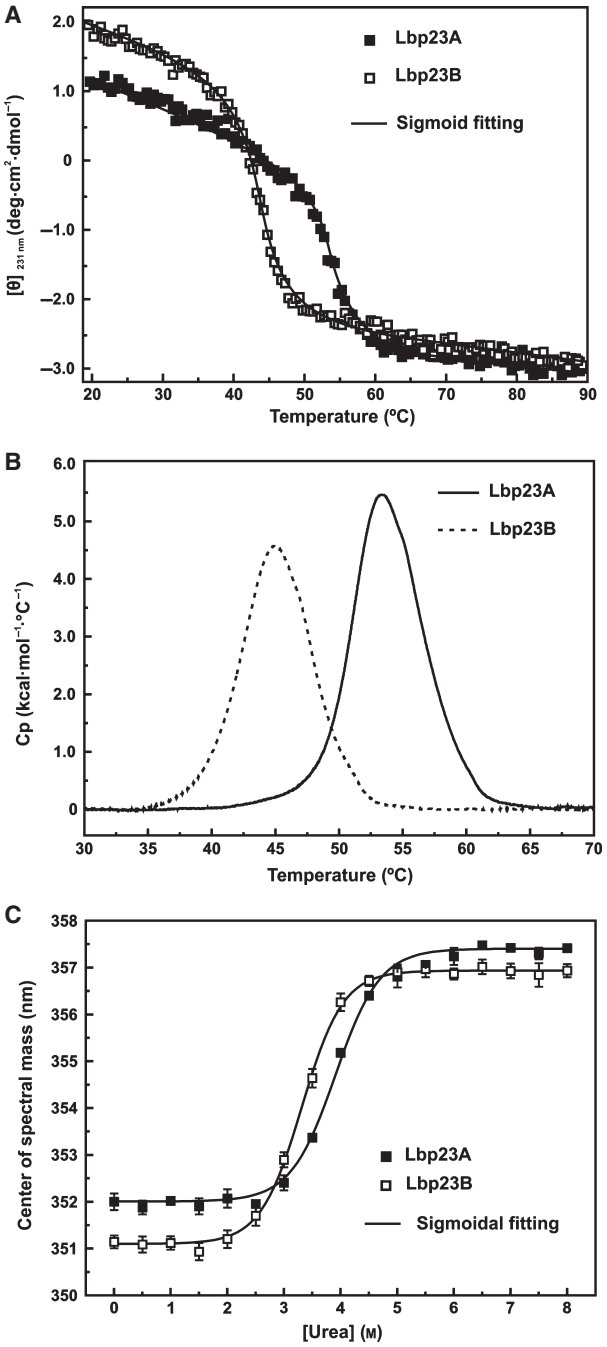

Fig. 5. Lbp23 thermal- and chemical-induced unfolding measurements. (A) Thermal-induced unfolding experiments performed using CD at 231 nm. The T_m values were estimated by sigmoidal fitting and are presented in Table 2. (B) Thermal-induced experiments performed using DSC. The figure shows only the first scan normalized to the heat capacity after subtraction of the buffer scanning and baseline treatment. The T_m values were estimated from the peak of the transition, as well as the ΔH^{cal}_{app} by application of Eqn (1) (Table 2). (C) Chemical-induced unfolding using urea as a chemical denaturant via measurements of the intrinsic fluorescence emission and analysis of the <λ>-signal (Table 2).

Table 2. Summary of Lbp23A and Lbp23B stability features.

		Protein	
Property	Technique	Lbp23A	Lbp23B
T_m (°C)	$CD_{231\ nm}$	53.0 ± 0.5	44.0 ± 0.5
	DSC	53.9 ± 0.2	45.1 ± 0.1
ΔH^{Cal}_{app} (kcal·mol^{-1})	DSC	115 ± 6	115 ± 4
C_m (mol·L^{-1})	Fluorescence	3.9 ± 0.1	3.3 ± 0.1

MDH aggregation under this condition (Fig. 6A). With luciferase as a model client protein, both Lbp23 proteins prevented thermal aggregation similarly (Fig. 6B) but with less efficiency than for MDH. These results indicated that the Lbp23 proteins have different intrinsic chaperone activity and can act on different *L. braziliensis* client proteins.

Hsp90 ATPase inhibition

Several studies noted that p23 is an inhibitor of Hsp90 ATPase activity [15,17]. Therefore, we investigated the effect of the Lbp23 isoforms on steady-state LbHsp90 ATPase activity. Figure 6C shows the dependence of the LbHsp90 ATPase activity on the concentration of the Lbp23 isoforms. Both proteins were capable of reducing the LbHsp90 ATPase activity but to different extents. Lbp23A inhibited the LbHsp90 ATPase activity by 50% (± 10%), whereas Lbp23B reduced it by approximately 20% (± 5%) at 30 μM (Fig. 6C); thus, although the behavior of the p23 isoforms is similar, the two proteins have particular features that distinguish them from each other.

The Lbp23 isoforms are cognate proteins in *L. braziliensis* promastigote cells

To investigate the presence of the Lbp23 proteins *in vivo*, we grew promastigote forms of antimony-sensitive and antimony-resistant *L. braziliensis* lines [33] at two temperatures (26 °C and 37 °C) and used polyclonal antibodies against the recombinant Lbp23 proteins. Under the tested conditions, cross-reactions between the antibodies and the recombinant proteins were not observed or were negligible (Fig. 7). As shown in Fig. 7, both native Lbp23 proteins were identified in the antimony-sensitive and antimony-resistant *L. braziliensis* lines and at the two tested growth temperatures. At 26 °C, native Lbp23A (Fig. 7A) was identified as a single band with a size similar to that of the recombinant protein, and no significant differences were observed for the growth times or tested lines. However, at 37 °C, the antimony-resistant line appears

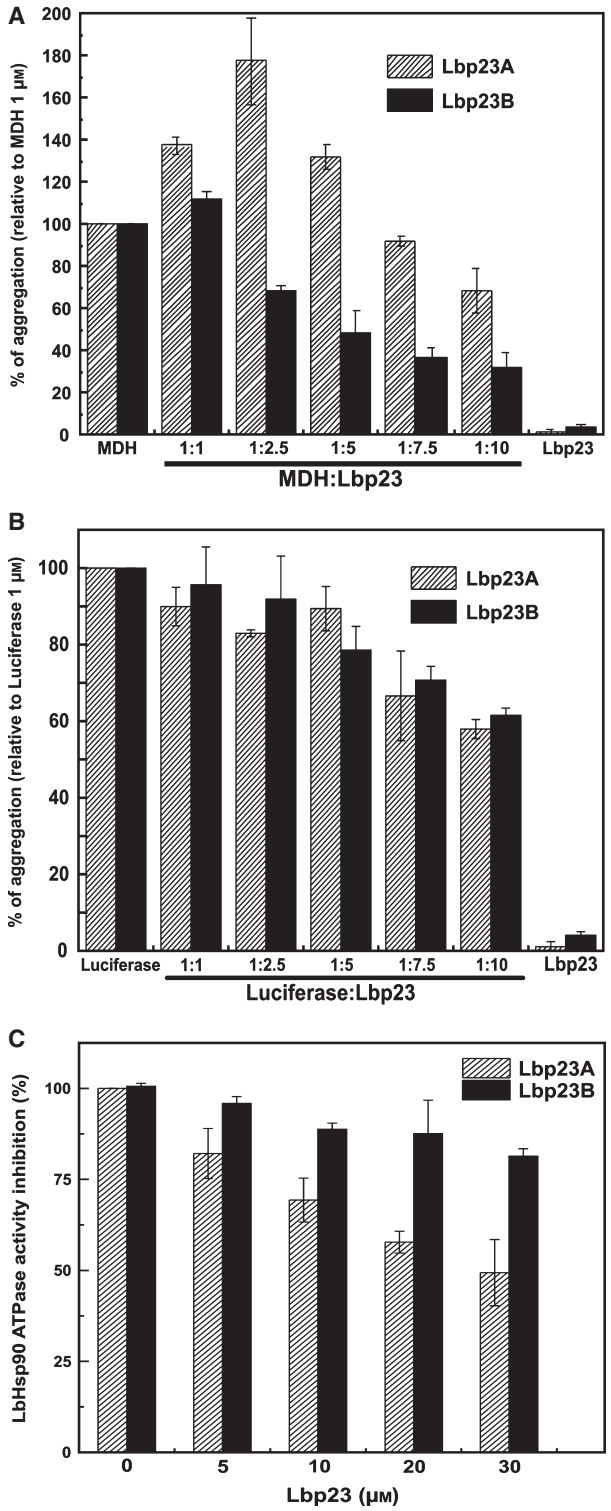

Fig. 6. Functional assays for Lbp23A and Lbp23B. Client proteins (1.0 μM), MDH (A) and luciferase (B), were incubated at 40 °C for 3 h with increasing amounts of Lbp23 to test the intrinsic chaperone activity of Lbp23A and Lbp23B. (C) LbHsp90 ATPase activity inhibition by Lbp23 protein concentration.

to show a higher amount of native Lbp23A (Fig. 7B). Lbp23B was also present in both lines that were grown at 26 °C, however, it underwent *in vivo* protein degradation; this reaction led to the identification of two bands with smaller MM (Fig. 7C). It is worth noting that, immediately after lyses of *L. braziliensis* cells grown at 26 °C, a band of similar size of the recombinant Lbp23B was observed (data not shown). Additionally, a weak band of size equivalent to the recombinant Lbp23B was observed when the image contrast was increased (data not shown). Taken together, these data indicate that the intact Lbp23B is present under these conditions and also suggested that natural Lbp23B suffer protein degradation. Interestingly, at 37 °C, two additional main bands of higher MM were also observed (Fig. 7D) for both lines and growth times, suggesting that Lbp23B may undergo some type of post-translational modification under this growth condition.

Lbp23 isoforms interact with LbHsp90 with similar affinities

The interaction between Lbp23 and LbHsp90 in the presence of ATP-γ-S was studied by isothermal titration calorimetry (ITC) (Fig. 8). Both binding reactions were exothermic and followed a stoichiometric ratio of one molecule of Lbp23 per dimer of LbHsp90. The measured K_D values of Lbp23A and Lbp23B for LbHsp90 were 0.7 ± 0.2 μM (Fig. 8A) and 1.1 ± 0.2 μM (Fig. 8B), respectively, and were therefore similar (inside the error), showing that both proteins have a high affinity for LbHsp90. Additionally, the apparent enthalpic and entropic contributions were almost the same for both cases ($\Delta H_{app} = -13.6 \pm 0.9$ kcal·mol^{-1}, $\Delta S_{app} = -16.6$ cal·mol^{-1}·deg^{-1} for Lbp23A and $\Delta H_{app} = -13.4 \pm 0.8$ kcal·mol^{-1}, $\Delta S_{app} = -16.8$ cal·mol^{-1}·deg^{-1} for Lbp23B), with the enthalpic component driving both interactions. As recently reported for the *L. braziliensis* Aha1 co-chaperone [34], the interaction of both Lbp23 proteins with LbHsp90 leads to a negative entropic change, suggesting a restriction in the freedom of the formed complex. Taken together, these thermodynamic data indicate that the interaction mechanism of the Lbp23 proteins with LbHsp90 is essentially the same, despite their low amino acid sequence identity.

We also analyzed the molecular masses and the interaction using sedimentation equilibrium-analytical ultracentrifugation (SE-AUC). Figure 9 shows the fitting of the SE data, demonstrating the good fit, as shown in the residuals panel (Fig. 9, bottom), as well as by the global reduced chi-squared. As a control, the three proteins were analyzed alone to confirm their oligomeric

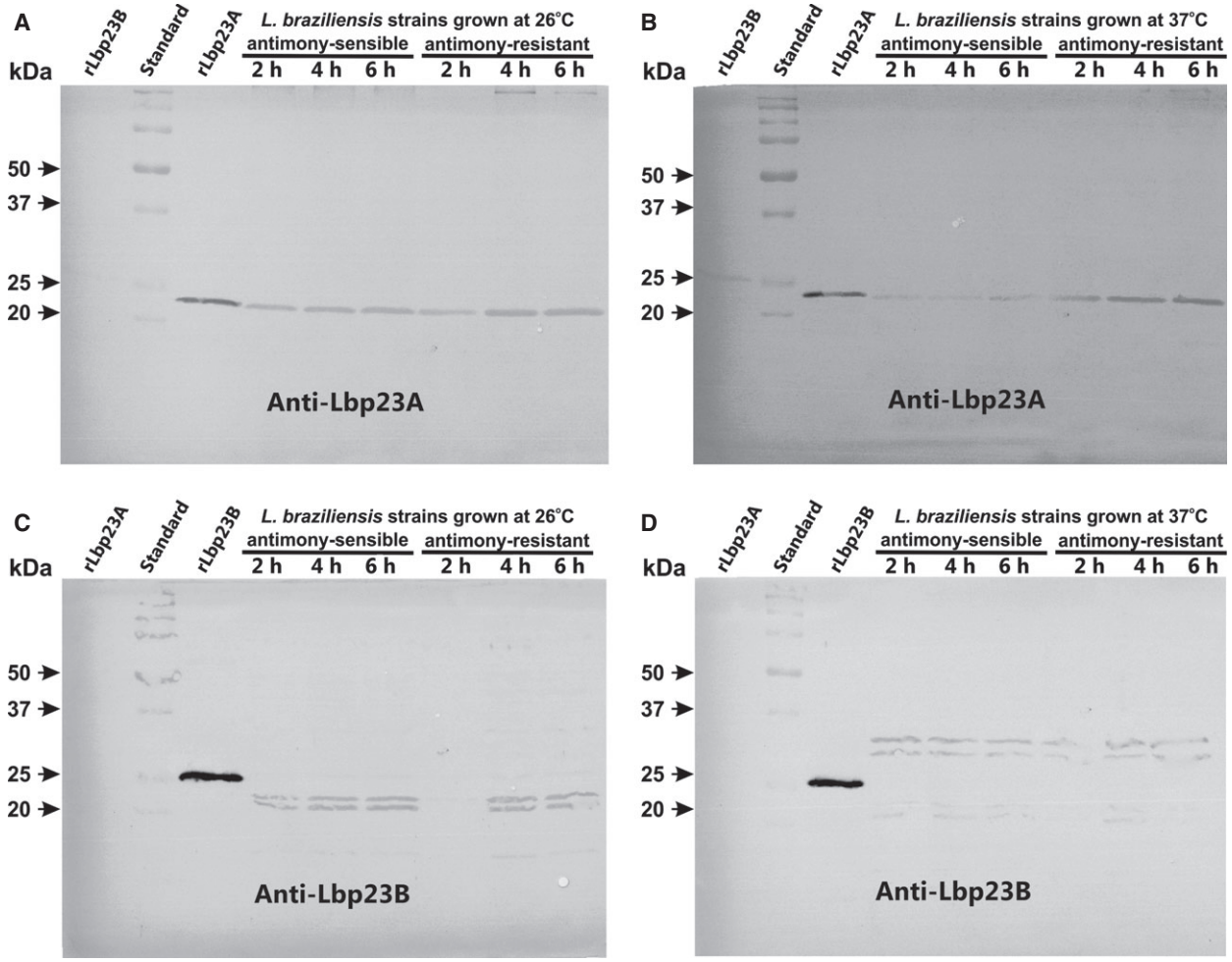

Fig. 7. Both Lbp23 proteins are cognate proteins in *L. braziliensis* promastigote cells. *L. braziliensis* promastigotes cells, both antimony-sensitive and antimony-resistant lines, grown for different periods (2, 4 and 6 h) and different temperatures (26 °C and 37 °C) were lysed and subjected to western blotting. (A) and (B) With the anti-Lbp23A antibody, one band of approximately 22 kDa was observed for all tested conditions; this band corresponded to the Lbp23A protein. Lane 1, recombinant Lbp23B; lane 2, molecular mass standard; lane 3, recombinant Lbp23A; lanes 4–9, lysates obtained under the conditions listed above. (C, D) With the anti-Lbp23B antibody, two bands of approximately 20 kDa (C) and 30 kDa (D) were displayed for all of the conditions tested; these bands corresponded to degradation products and probable post-translationally modified Lbp23B species. Lane 1, recombinant Lbp23A; lane 2, molecular mass standard; lane 3, recombinant Lbp23B; lanes 4–9, lysates obtained under the conditions listed above. Arrows indicate the standard molecular mass.

status. Considering the MM obtained for each protein (Table 3), we concluded that both Lbp23 proteins were in the monomeric state (Fig. 9A,B), thus confirming the aforementioned SV experiments. The SE data obtained for LbHsp90 indicated that it behaved as a dimer of 165 ± 2 kDa (Fig. 9C). However, as shown previously, LbHsp90 forms a monomer–dimer equilibrium with a K_D of approximately 80 nM [35]. Treating the obtained data as a self-association model resulted in an LbHsp90 dimer–monomer K_D of 65 ± 5 nM (Fig. 9D), which is similar to that reported previously [35]. Therefore, at the LbHsp90 concentrations tested, the protein was more than 99.5% dimeric. Using the same conditions for the experiments on the interaction between LbHsp90 and Lbp23 proteins and considering the stoichiometry of one Lbp23 molecule per LbHsp90 dimer (Eqn 4), we obtained a K_D of 8.1 ± 0.7 μM for the LbHsp90/Lbp23A complex (Fig. 9E) and 10.7 ± 0.3 μM for the LbHsp90/Lbp23B complex (Fig. 9F). These constants are one order of magnitude higher than those obtained by ITC, which can be explained by the absence of adenosine nucleotides in the AUC experiments; this absence decreased the affinity of Lbp23 for Hsp90 [15,36].

To confirm the influence of nucleotides on these interactions, the K_D values for Lbp23A and Lbp23B

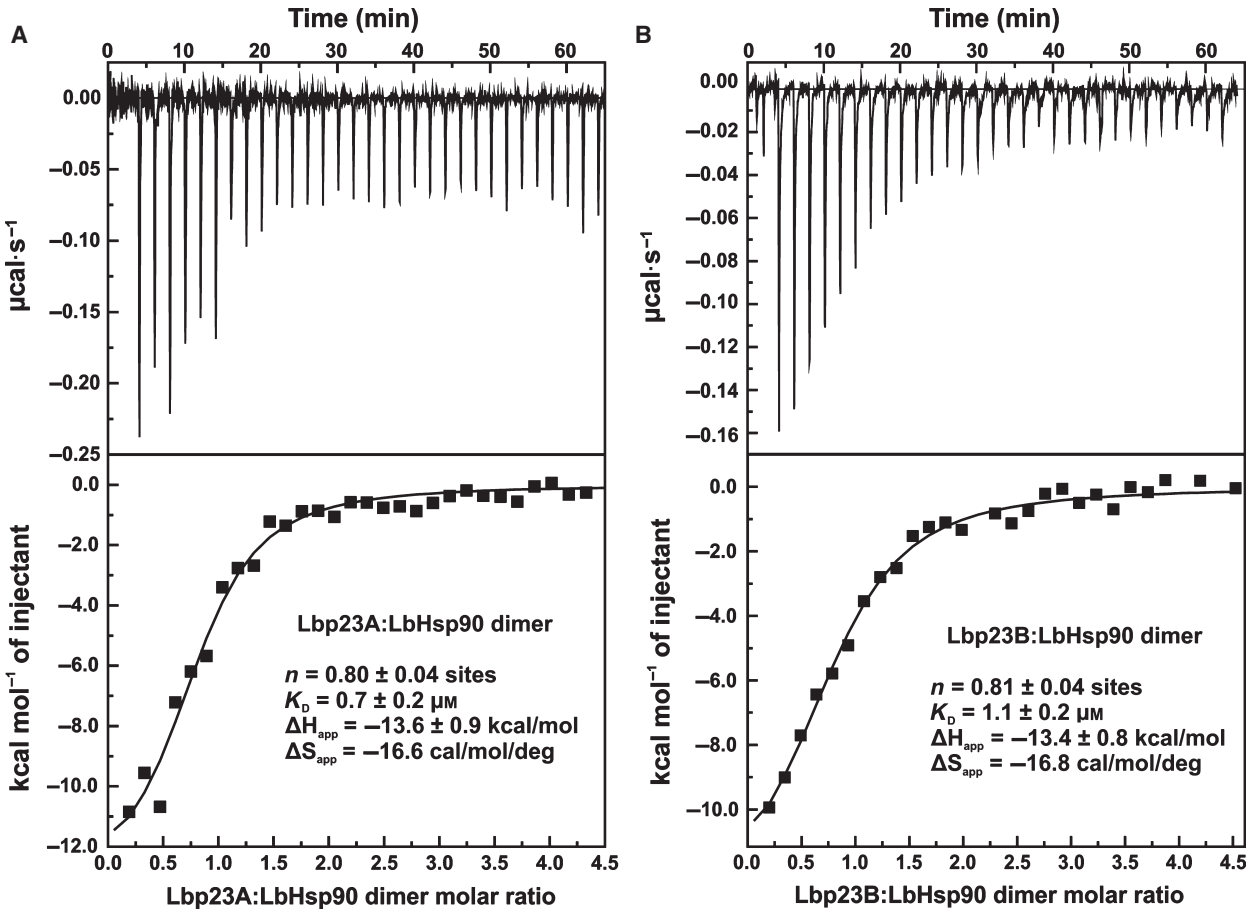

Fig. 8. ITC measurements of the interaction between LbHsp90 and Lbp23. Curves for the isothermal titrations (at 30 °C) of approximately 150 µM (A) Lbp23A or (B) Lbp23B into 5 µM LbHsp90 dimers in the presence of 2 mM ATP-γ-S. Thermodynamic parameters were derived from nonlinear least-squares fitting.

and LbHsp90 were determined using the same technique based on the change in anisotropy of fluorescein-labeled Lbp23 after the formation of the protein–protein complex. Lbp23A showed a K_D of 4.8 ± 0.1 µM and 2.9 ± 0.1 µM in the absence and presence of ATP, respectively (Fig. 10A). Similarly, Lbp23B presented a K_D of 11.1 ± 0.1 µM and 3.3 ± 0.1 µM in the absence and presence of ATP, respectively (Fig. 10B). As shown by the ITC data, both Lbp23 proteins showed higher affinity for LbHsp90 in the presence of ATP or its analogue, although the interaction does occur even in the absence of an adenosine nucleotide, as shown by the AUC.

Although the constants from the different techniques are within the same order of magnitude, the K_D values obtained by fluorescence anisotropy are slightly higher, indicating an interaction that shows lower affinity compared to that for the K_D obtained by ITC and AUC. This result might possibly be a result of the labeling of the Lbp23 proteins with FITC, which could have diminished the complex affinity. This effect was observed previously [37] and, although the effect has translated into a somewhat different K_D, it did not prevent the use of the technique to confirm the interaction between proteins. The only exception to this observation occurred for the interaction between Lbp23A/LbHsp90 in the absence of nucleotide (K_D of 4.8 ± 0.1 µM by fluorescence versus a K_D of 8.1 ± 0.7 µM by AUC). In addition to these considerations, it is worth noting that the K_D is calculated based on a set of assumptions for each method. Therefore, the K_D values can vary depending on the adopted methodology; however, the variation is within an acceptable range, particularly when comparing direct and indirect measurements.

Discussion

Molecular chaperones of the Hsp90 family are found in several organisms, including protozoa. The Hsp90

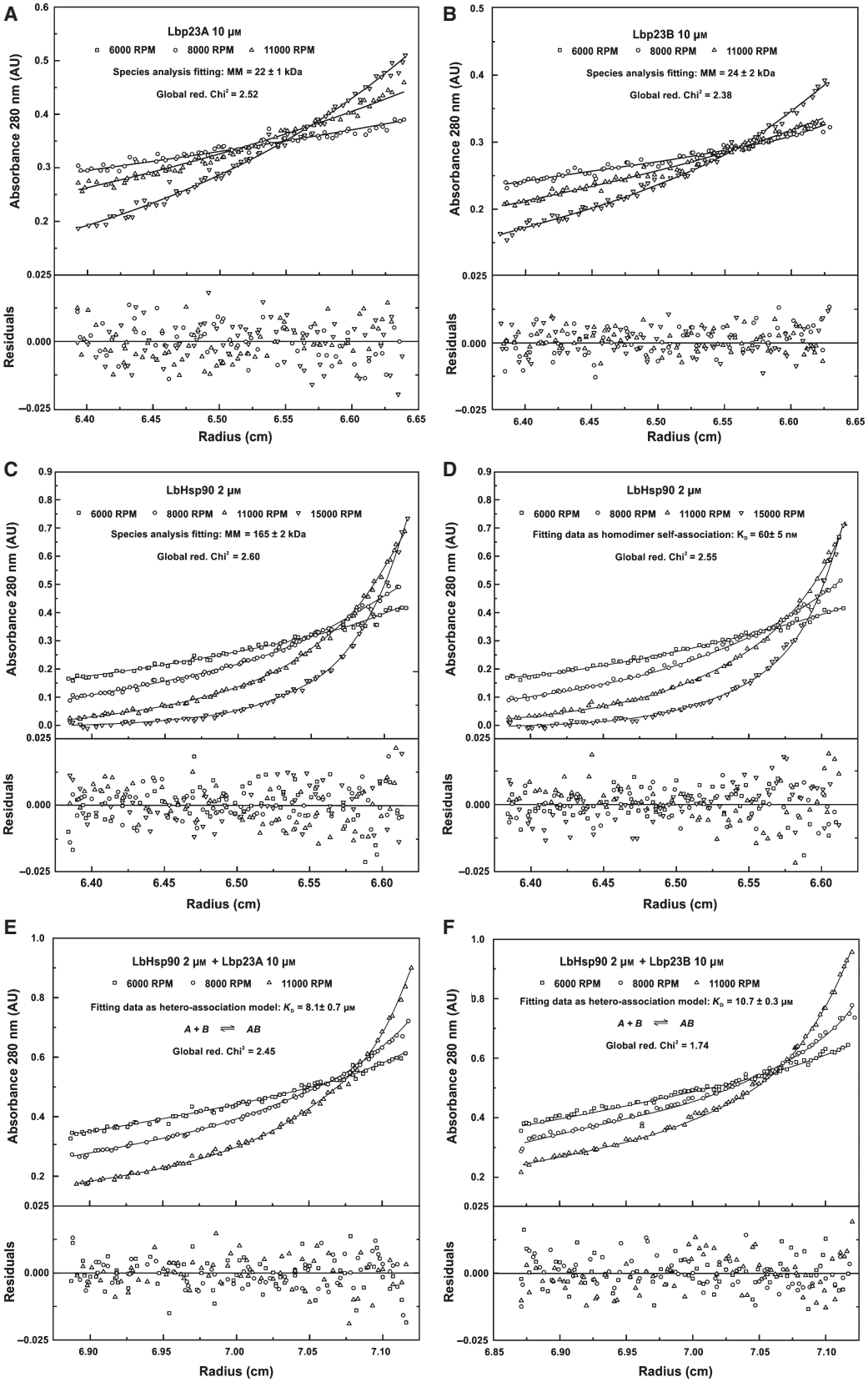
A
Lbp23A 10 μM
6000 RPM 8000 RPM 11000 RPM
Species analysis fitting: MM = 22 ± 1 kDa
Global red. Chi² = 2.52
B
Lbp23B 10 μM
6000 RPM 8000 RPM 11000 RPM
Species analysis fitting: MM = 24 ± 2 kDa
Global red. Chi² = 2.38
C
LbHsp90 2 μM
6000 RPM 8000 RPM 11000 RPM 15000 RPM
Species analysis fitting: MM = 165 ± 2 kDa
Global red. Chi² = 2.60
D
LbHsp90 2 μM
6000 RPM 8000 RPM 11000 RPM 15000 RPM
Fitting data as homodimer self-association: K_D = 60± 5 nM
Global red. Chi² = 2.55
E
LbHsp90 2 μM + Lbp23A 10 μM
6000 RPM 8000 RPM 11000 RPM
Fitting data as hetero-association model: K_D = 8.1± 0.7 μM
A + B ⇌ AB
Global red. Chi² = 2.45
F
LbHsp90 2 μM + Lbp23B 10 μM
6000 RPM 8000 RPM 11000 RPM
Fitting data as hetero-association model: K_D = 10.7 ± 0.3 μM
A + B ⇌ AB
Global red. Chi² = 1.74
Absorbance 280 nm (AU)
Residuals
Radius (cm)

Fig. 9. Sedimentation equilibrium data for Lbp23 proteins, LbHsp90 and LbHsp90-Lbp23 complexes. Summary of the sedimentation equilibrium data fitting for Lbp23A (A), Lbp23B (B) and LbHsp90 (C) by the 'species analysis' model of SEDPHAT, suggesting that Lbp23 proteins behaved as monomers, whereas LbHsp90 was dimeric. LbHsp90 data was also fitted by the self-association model (D) indicating a dimer–monomer equilibrium with K_D of 65 ± 5 nM. The complex Lbp23A-LbHsp90 (E), in the absence of adenosine nucleotide, indicated a K_D of 8.1 ± 0.7 μM, whereas the complex Lbp23B-LbHsp90 (F) showed a K_D of 10.7 ± 0.3 μM. The fitting goodness can be evaluated in the residuals panel (bottom panel) as well as by the global reduced chi-squared values. In all cases, the global fitting was performed in multispeed equilibrium data mode with at least two protein concentrations. For space restriction questions, the fitting curves for only one protein concentration are presented.

Table 3. Interaction properties of Lbp23 proteins with LbHsp90 obtained by SE experiments.

	Species analysis		Association model	
Sample	MM (kDa)	Chi-squared	K_D (μM)	Chi-squared
Lbp23A	22 ± 1	2.52	–	–
Lbp23B	24 ± 2	2.38	–	–
LbHsp90	165 ± 2	2.60	0.060 ± 0.005[a]	2.55
Lbp23A + LbHsp90	–	–	8.1 ± 0.7[b]	2.45
Lbp23B + LbHsp90	–	–	10.7 ± 0.3[b]	1.74

[a]Self-association model.
[b]Hetero-association model.

proteins are known for having a mechanical cycle that is guided by ATP binding and hydrolysis, which involves several large conformational changes [35]. Several studies have shown that this molecular mechanism is controlled by the Hsp90 co-chaperones, as well as post-translational modifications [2].

We have studied the Hsp90 protein, as well as its co-chaperones, in *L. braziliensis* to identify the features that are related to the protein functional cycle and inhibition. Among the identified Hsp90 co-chaperones, we found two putative p23s in the *L. braziliensis* genome [4,38]. Using the primary structure, we observed that, despite the low identity between them and with hp23, they do present the motif corresponding to p23 proteins [9]. Searches in the public genome databases led to the identification of two orthologous p23s in several other trypanosomatids. These proteins were organized into two large groups as orthologues of hp23 and of Sba1, suggesting that they are conserved in these organisms. The presence of two p23s in different organisms in which the life cycle encompass a transition from an insect to a mammalian host, but not in organisms with only one stage of life, such as *Caenorhabditis elegans*, *Drosphila melanogaster*, *Danio rerio*, *Xenopus tropicalis*, *Gallus gallus*, *Bos taurus*, *Rattus norvegicus* and *Schizosaccharomyces pombe* (data not shown), suggests that the existence of two p23s may be a regulatory or adaptive mechanism related to the environmental differences experienced by these species during their life time. One can easily speculate that each p23 might be more active or stable in one host than in another. It is also still possible that they have different mechanisms of interaction with Hsp90. These possibilities initially guided our experiments.

To explain the presence of two p23 proteins in trypanosomatids, we produced the recombinant proteins for structural characterization and found a similar secondary structure content for the two proteins. They also have a positive CD signal at 230 nm, which is a structural sign reported for the hp23 protein [8,11]. In addition, we used hydrodynamic tools to show that both Lbp23 proteins are elongated monomers in solution, similar to the observations for hp23 [39]. SAXS experiments corroborate these conclusions and indicate that both Lbp23 proteins have sufficiently long dimensions to interact simultaneously with both the N- and M-domains of LbHsp90 [39].

Despite the structural similarity between the Lbp23A and Lbp23B proteins, they showed quite different stabilities under denaturing conditions. The presence of two p23 isoforms in protozoa with different stabilities, as observed in the present study, immediately suggested that the isoforms can perform different roles *in vivo*. Recently, it was shown that the yeast Sba1 has a large network of *in vivo* interactions, which are both dependent and independent of Hsp90 [40]. Therefore, we functionally characterized Lbp23. Our results suggested that both Lbp23 proteins have intrinsic chaperone

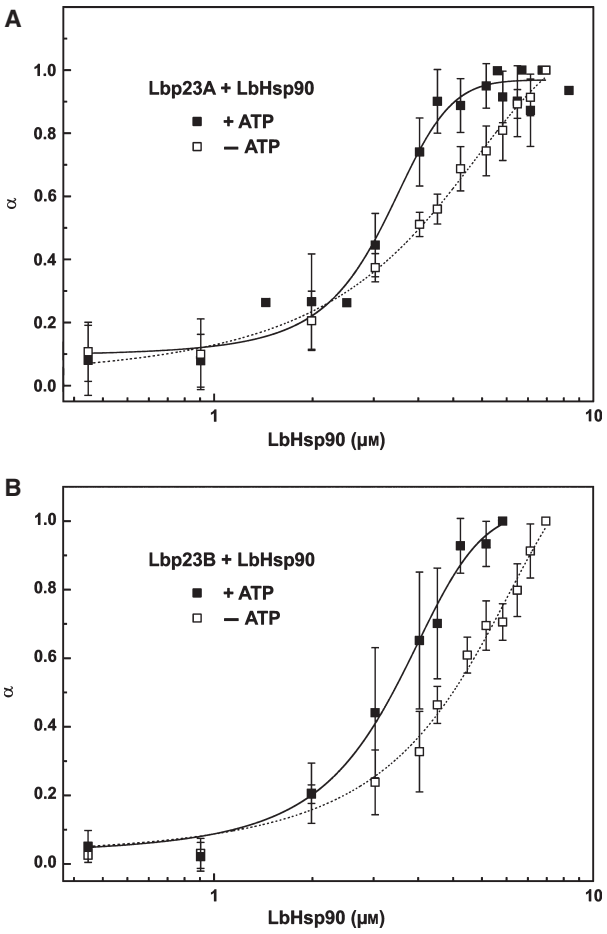

Fig. 10. Fluorescence anisotropy assay to determine the K_D of the interaction between LbHsp90 and the Lbp23 proteins. Fluorescence anisotropy curves were obtained in the presence or absence of 5 mM ATP at 30 °C and increasing concentrations of LbHsp90, using 15 nM FITC-labeled (A) Lbp23A or (B) Lbp23B. The samples were excited at 495 nm, and the emission components were collected through a long-pass (> 520 nm) filter. K_D values were obtained by fitting the experimental data using GRAPHPAD PRISM, version 5.

activity; however, they acted differently on the tested model client proteins and therefore may specifically interact with different client proteins in *L. braziliensis* cells. Moreover, both Lbp23 proteins also inhibited LbHsp90 ATPase activity but to a different extent. Lbp23A inhibited the LbHsp90 ATPase activity by almost 50%, whereas Lbp23B only inhibited the activity by approximately 20%.

We also performed western blot experiments to identify the *in vivo* presence of Lbp23 proteins in promastigote forms of *L. braziliensis* at two temperatures. We also tested pentavalent antimony-sensitive and pentavalent antimony-resistant *L. braziliensis* lines [33]. First, our results led to the identification of both Lbp23 isoforms at all tested conditions, indicating that these p23 proteins are cognate proteins. It was demonstrated recently that one of protein spots identified as being more abundant in the antimony-resistant *L. infantum* line corresponded to p23 [41], supporting the reliability of the results reported in the present study. However, Lbp23B appears to undergo protein degradation and may suffer from some post-translation modifications when grown at 37 °C. A search for phosphorylation sites on the Lbp23 primary structures showed that both proteins possess several sites with a high probability of being phosphorylated (data not shown). Interestingly, in protozoa, Hsp90 post-translational modifications, such as acetylation and phosphorylation, appear to play an important role in regulating the assembly of the Hsp90 complex [28,29], and Hsp90 becomes phosphorylated after temperature adaptation [29]. Furthermore, in *Plasmodium falciparum*, the p23 orthologue is phosphorylated in the trophozoite forms [42]. Similarly, a systematic study confirmed that the hp23 protein is also the target of phosphorylation by casein kinase II [43]. Taken together, these observations indicate that native Lbp23B may be phosphorylated when *L. braziliensis* lines are grown at 37 °C. However, more detailed experiments must be performed to understand the post-translational modifications of Lbp23 proteins. Moreover, these *in vivo* results may indicate divergent cellular roles for these proteins.

Because the presence of two p23 proteins was confirmed *in vivo* and knowing that the two proteins have different physicochemical properties, we searched for the interaction parameters between the two proteins and LbHsp90. Our ITC results indicate that one Lbp23 molecule binds to an LbHsp90 dimer, which is in agreement with the results previously obtained for other organisms [17,36]. The K_D values obtained in the presence of a nonhydrolyzable adenosine nucleotide analogue indicate that LbHsp90 has a similar affinity for the Lbp23A and Lbp23B proteins. Interestingly, the thermodynamic parameters suggested that the Lbp23 proteins share a similar mechanism for interaction with LbHsp90; the interaction for both proteins is enthalpically driven but has unfavorable entropy. This entropic penalty is most likely a result of restriction of the LbHsp90 freedom, similar to that observed for the interaction between LbAha1 and LbHsp90 [34], and is consistent with the dimerization of the Hsp90 N-domains [12,13]. Considering all of the structural results reported above, the similarity of the mechanism for the interaction of the Lbp23 proteins with LbHsp90 is not unexpected, despite the low amino acid sequence identity.

The interaction of p23 proteins with Hsp90 is modulated by the presence of adenosine nucleotides [15]. Because the interactions between the Lbp23 proteins and LbHsp90 in the absence of adenosine nucleotides were not detectable by ITC experiments, we used SE-AUC (Fig. 9) to test this condition. This methodology was also used to confirm that the Lbp23 proteins behave as monomers with no detectable oligomerization behavior. We also observed that, for the tested LbHsp90 concentration, more than 99.5% of LbHsp90 is a dimer. Interestingly, even in the absence of an adenosine nucleotide, LbHsp90 has a K_D for the Lbp23 proteins in the micromolar range (Table 3), demonstrating high affinity; however, it was one order of magnitude lower than the K_D in the presence of an adenosine nucleotide analogue, as measured by ITC (Fig. 8).

The AUC device used does not allow for analysis of interactions in the presence of high concentrations of adenosine nucleotide; thus, we employed the versatility of the fluorescence anisotropy methodology to measure the affinity of the interactions in the presence and absence of ATP. Even with this approach, both Lbp23 proteins showed similar and higher affinities for LbHsp90 in the presence of ATP.

The results reported in the present study demonstrate that, even with their low degree of identity, the two p23s that are found in *L. braziliensis* are able to interact with Hsp90, following a similar mode of interaction with similar affinities. Thus, it is important to note that, although both proteins interact similarly with LbHsp90, they exhibit distinct chemical and thermal stability profiles, as well as slight differences in their intrinsic chaperone and LbHsp90 ATPase inhibition activities.

These proteins belong to a parasite that has two distinctive stages during its life cycle. Using western blot analysis, we observed some differences in the Lbp23A and Lbp23B expression profiles. These differences, which are associated with their divergent physicochemical and functional characteristics, suggest that the presence of two p23s in *L. braziliensis* may be related to the possibility for parasite adaptation to the various conditions encountered during its digenetic life cycle.

In conclusion, the present study unequivocally demonstrates the existence of two p23 isoforms in *L. braziliensis*, as well as in other trypanosomatids. Furthermore, our experimental observations indicate that Lbp23A and Lbp23B may show distinct activities in regulating LbHsp90 and that the *L. braziliensis* Hsp90 system has traits possibly allowing for new forms of selective inhibition of the protozoan Hsp90. Despite these results, many questions remain with respect to understanding the role of two p23s in trypanosomatids. Future functional studies will aim to shed light on the function of Lbp23.

Experimental procedures

Protein identification and sequence analysis

The search for Lbp23 was performed using the hp23 sequence (dBEST reference: 4704885) in BLASTP against the *L. braziliensis* genome sequence database. The sequence alignment between Lbp23A (Protein ID: XP_001568545.1; GenBank accession number: LbrM.34.4450), Lbp23B (Protein ID: XP_001564309.1; GenBank accession number: LbrM.20.0220) and hp23 was analyzed using CLUSTALW2 [44]. Our searches also revealed two p23 proteins in two other Plasmodiidae family species and six Trypanosomatidae family species, allowing a multiple sequence alignment and the construction of a dendrogram based on established methods using CLUSTALW2.

Cloning, expression and purification

The DNA encoding Lbp23A and Lbp23B was amplified by PCR using the genomic DNA from *L. braziliensis* M2904 (MHOM/BR/75/M2904) and specific primers (data not shown). This strategy allowed the construction of pET28a::Lbp23A and pET28a::Lbp23B vectors, which were used to express recombinant proteins that contained a His-tag at the N-terminal. The Lbp23A and Lbp23B cloning was confirmed by automated DNA sequencing (data not shown).

The Lbp23A recombinant protein was expressed in the *Escherichia coli* BL21(DE3) strain (at 37 °C) and Lbp23B was expressed in the *E. coli* BL21(DE3) pLysS strain (at 30 °C). The bacterial cells were disrupted by sonication and centrifuged at 15 550 ***g***. for 30 min at 4 °C. The proteins were purified by Ni^{2+}-affinity chromatography and incubated with 1 $U \cdot mg^{-1}$ of thrombin (Sigma, St Louis, MO, USA) for His-tag cleavage. The last step of purification was performed using size exclusion chromatography onto a Superdex 200 26/60 column. The purity was checked by 12% SDS/PAGE. LbHsp90 was produced as described previously [35]. The protein concentration was determined spectrophotometrically using the calculated extinction coefficient for the denatured proteins, as estimated by SEDNTERP (http://www.jphilo.mailway.com/download.htm).

Spectroscopy studies

CD measurements were performed in a Jasco J-815 spectropolarimeter and the temperature was controlled by a Peltier-type PFD 425S system (Jasco Inc., Easton, MD, USA). The CD spectra were acquired using a 0.2-mm path length cuvette containing 600 $\mu g \cdot mL^{-1}$ protein in a buffer contain-

ing 25 mM Tris-HCl (pH 7.5), 100 mM NaCl and 1 mM β-mercaptoethanol. All CD data were displayed as mean [θ]. Intrinsic fluorescence emission measurements were performed in an F-4500 Fluorescence Spectrophotometer (Hitachi, Tokyo, Japan) using a 1 x 0.2-cm path length cuvette with 2.5 μM protein in the aforementioned buffer. The data were analyzed using (λ):

$$<\lambda> = \Sigma\lambda_i F_i/\Sigma F_i \quad (1)$$

where λ_i is the wavelength measured and F_i is the fluorescence intensity at λ_i. Thermal- and chemical-induced unfolding experiments were conducted as reported previously [34].

DSC

DSC experiments were performed using a Nano DSC (TA Instruments, Newcastle, DE, USA) and the measurements were performed at protein concentrations of approximately 1.1–1.4 mg·mL^{-1} after extensive dialysis against a buffer containing 25 mM Tris-HCl (pH 7.5) and 100 mM NaCl. The heating rate was 1 °C·min^{-1} for the temperature ranging from 15 °C to 90 °C. The experimental data were processed with NANO ANALYZE (TA Instruments), which provided the T_m, for which the baselines were calculated from the pre- and post-transition temperature regions. The apparent calorimetric enthalpy change of the unfolding transition (ΔH_{app}^{cal}) was calculated by integrating the heat capacity (Cp^{trs}) during the heating:

$$\Delta H_{app}^{cal} = \int_{T1}^{T2} Cp^{trs} dT \quad (2)$$

where T is the temperature (K).

Hydrodynamic characterization

aSEC experiments and R_S determination were performed as described previously [34].

SV-AUC experiments were conducted in a Beckman Optima XL-A analytical ultracentrifuge (Beckman Coulter, Fullerton, CA, USA) at Lbp23 concentrations ranging from 100 to 800 μg·mL^{-1} in 25 mM Tris-HCl (pH 7.5) containing 100 mM NaCl and 1 mM β-mercaptoethanol at 20 °C at 129 024 ***g***, with data acquisition at 280 nm. The experimental absorbance data were fitted by SEDFIT, version 12.1 [45], where the f/f_0 parameter served as a regularization parameter for the fitting equation. The experimental sedimentation coefficients (s) were found as the maximum of the peaks of the distribution function of the sedimentation coefficient $c(S)$ curves, after normalization to standard conditions ($s_{20,w}$). The standard sedimentation coefficient at 0 mg·mL^{-1} protein concentration ($s^0_{20,w}$), which is an intrinsic parameter of the particle [46], was estimated by linear regression of the curve of the $s_{20,w}$ value as a function of the protein concentration. SEDFIT estimated the $s_{20,w}$ value based on information about the buffer viscosity (η = 0.010185), buffer density (ρ = 1.00307 g·mL^{-1}) and partial-specific volume of each studied protein (V_{bar}: Lbp23A = 0.720 cm^3·g^{-1}; Lbp23B = 0.725 cm^3·g^{-1}) which were supplied by SEDNTERP.

SAXS

SAXS experiments were performed at the SAXS2 beamline in the Laboratório Nacional de Luz Síncrotron (LNLS, Campinas-SP, Brazil). The X-ray scattering data were acquired using a two-dimensional MARCCD detector (Rayonix, LLC, Evanston, IL, USA). The measurements were performed with a monochromatic X-ray beam (wavelength of λ = 1.488 Å) and a sample-to-detector distance of approximately 1000 mm, corresponding to a scattering vector range of $0.015 < q < 0.35$ Å^{-1}, where q is the magnitude of the q-vector defined by $q = (4\pi/\lambda)\sin\theta$ (2θ is the scattering angle). Lbp23A and Lbp23B protein samples were placed in a 1-mm path length cell, and the scattering patterns were recorded at different sample concentrations (approximately 1.0, 2.0 and 4.0 mg·mL^{-1} in a buffer containing 25 mM Tris-HCl (pH 8.0) with 100 mM NaCl and 5 mM β-mercaptoethanol). The samples and the buffer were recorded using 300-s frames. The scattering curves were corrected for the attenuation of the samples, and the buffer scattering curve was subtracted from the corresponding scattering curve for the sample. The samples were also checked for radiation damage by measuring consecutive frames. Protein aggregation was checked using the Guinier approximation [linearity in the Ln $I(q) \times q^2$ plot, for small q values) and the R_g values were also estimated [47]. $p(r)$ values were calculated using GNOM [48]. The *ab initio* models of the Lbp23 proteins were constructed using DAMMIN [49], and at least 20 models were averaged using the DAMAVER [47–50], leading to the final *ab initio* models. HYDROPRO [51] was used for the averaged structures to calculate the hydrodynamic properties and validate the generated low-resolution structures.

Chaperone activity

The chaperone activities of Lbp23A and Lbp23B were tested as their ability to prevent protein aggregation. Samples containing 1 μM MDH or 1 μM luciferase in the absence and presence of increasing concentrations of Lbp23A or Lbp23B (1–10 μM) were incubated for 3 h at 40 °C in Tris-HCl buffer (pH 7.5) containing 100 mM NaCl and 1 μM β-mercaptoethanol. The protein aggregation was measured in terms of light scattering at 320 nm. The aggregation propensity of Lbp23A and Lbp23B was also tested at the described temperature and 10 μM. Light scattering from controls containing only MDH or luciferase after 3 h of incubation at 40 °C was set as 100%.

LbHsp90 ATPase inhibition measurements

The inhibitory effects of Lbp23A and Lbp23B on the LbHsp90 ATPase activity were measured via the enzyme kinetics using an EnzChek Phosphate Assay kit (Invitrogen, Carlsbad, CA, USA), as described previously [35]. Briefly, LbHsp90 (1 μM dimer) was incubated in a 96-well microplate at 37 °C with 1.0 mM ATP and 5 mM $MgCl_2$ in the presence of increasing concentrations of Lbp23A and Lbp23B (0–30 μM). All samples were prepared in 40 mM Hepes (pH 7.5) buffer containing 100 mM KCl. The hydrolyzed P_i was quantified as described above, and the ATP hydrolysis rate at each Lbp23 protein concentration was converted into the relative ATPase activity. The data were expressed as a percentage of inhibition.

Parasite growth, protein extraction and western blot analysis

For *in vivo* detection of both Lbp23 proteins, we used sensible and antimony-resistant *L. braziliensis* (MHOM/BR/75/M2904) lines. This SbIII-resistant line was previously *in vitro* selected by continuous stepwise drug pressure with SbIII [33]. Parasites were grown at 25 °C and 37 °C several times and the protein preparation was performed as described previously [34]. Western blot analysis was performed on a 0.22-μm nitrocellulose membrane using rabbit-produced polyclonal primary antibodies against the recombinant Lbp23A (dilution 1 : 25 000) and Lbp23B (dilution 1 : 25 000) proteins (Célula B – Serviço de Produção de Anticorpos, Porto Alegre, Brazil) and goat anti-rabbit IgG alkaline phosphatase-conjugated secondary antibodies (dilution 1 : 30 000) (Sigma). For staining, a method based on alkaline phosphatase and NBT/BCIP reagents was used [34].

Interaction studies

ITC experiments were performed at 30 °C in an iTC200 microcalorimeter (GE Healthcare, Milwaukee, WI, USA). All proteins were dialyzed extensively against 40 mM Hepes buffer (pH 7.5) containing 20 mM KCl (Lbp23A) or 100 mM KCl (Lbp23B), 5 mM $MgCl_2$ and 1 mM β-mercaptoethanol. Aliquots of each Lbp23 at approximately 150 μM were injected into 5 μM LbHsp90 (dimeric species) in the presence of 2 mM ATP-γ-S (Sigma). The data were analyzed with ORIGIN (MicroCal, Inc., Northampton, MA, USA) using the one set of sites model to calculate the apparent binding enthalpy change (ΔH_{app}), binding stoichiometry (n) and association constant (K_A). The apparent Gibbs energy (ΔG_{app}) and apparent binding entropy change (ΔS_{app}) were calculated using:

$$\Delta G_{app} = -RT\ln K_A = \Delta H_{app} - T\Delta S_{app} \quad (3)$$

where R is the gas constant ($cal{\cdot}K^{-1}{\cdot}mol^{-1}$) and T is the absolute temperature (K). The dissociation constant (K_D) was considered as $1/K_A$.

SE experiments were performed at 20 °C to study the interaction of 2 μM LbHsp90 (dimer concentration) with Lbp23 proteins at increasing concentrations (2, 5 and 10 μM). As controls, SE experiments were performed for LbHsp90 (2 and 5 μM), Lbp23A (5 and 10 μM) and Lbp23B (5 and 10 μM) separately. To determine whether Lbp23A interacts with Lbp23B, the mixture of these proteins (5 and 10 μM) was also subjected to SE experiments. All proteins were prepared in 40 mM Hepes buffer (pH 7.5) containing 100 mM KCl, 5 mM $MgCl_2$ and 1 mM β-mercaptoethanol and were exhaustively dialyzed. The proteins were subjected to sedimentation at 2903 ***g***, 5161 ***g***, 9757 ***g*** and 18 144 ***g***. and scan data were acquired after 12 h of centrifugation at each speed. SE analysis involved fitting of the absorbance (at 280 nm) versus cell radius data using a nonlinear regression routine implemented in the SEDPHAT, version 10.58d [52]. The distribution of the protein along the cellwas fitted to the following equation for an associating system [53]:

$$C = C_{r_0} e\left[\frac{MM(1 - V_{bar}\rho)\omega^2\left(r^2 - r_0^2\right)}{2RT}\right] \quad (4)$$

where C is the protein concentration at the radial position r, C_{r0} is the protein concentration at the radial position r_0 (initial radial position) and ω is the centrifugal angular velocity. The 'species analysis' model was used to estimate the MM of both Lbp23 proteins. As previously shown, the LbHsp90 dimer dissociates into monomers [35]; then, the self-association method was used to analyze the LbHsp90 SE experiments.

A hetero-association model, as described by Eqn (4), was used to fit the sedimentation equilibrium data that was obtained for the Lbp23-LbHsp90 complexes.

$$A + B \rightleftharpoons AB \quad (5)$$

Equation 4 can be developed for equilibrium systems with more species, giving rise to Eqn (6):

$$C = C_{monomer,\,r_0} e\left[\frac{MM(1 - V_{bar}\rho)\omega^2\left(r^2 - r_0^2\right)}{2RT}\right] + K_A\left(C_{monomer,\,r_0}\right)^n e\left[\frac{MM(1 - V_{bar}\rho)\omega^2\left(r^2 - r_0^2\right)}{2RT}\right] \quad (6)$$

The predicted MM and molar absorbance of each folded protein at 280 nm was estimated by SEDNTERP as: LbHsp90 – 165 686 Da and 114 600 $L{\cdot}mol^{-1}{\cdot}cm^{-1}$, respectively; Lbp23A – 22 090 Da and 31 970 $L{\cdot}mol^{-1}{\cdot}cm^{-1}$, respectively; and Lbp23B – 23 045 Da and 29 450 $L{\cdot}mol^{-1}{\cdot}cm^{-1}$, respectively. All of these parameters were used in SEDPHAT software for hetero-association fitting. For all data sets, all parameters were allowed to float freely,

and the statistical analyses were performed using Monte Carlo nonlinear regression; with 1000 iterations and a confidence level of 0.68.

Fluorescence anisotropy measurements were performed using 15 nM FITC-labeled Lbp23A or Lbp23B in 20 mM potassium phosphate buffer (pH 7.5) containing 50 mM potassium chloride, 0.1% Tween 20, 2% glycerol, 1 mM EDTA and 1 mM β-mercaptoethanol in the presence or absence of 5 mM ATP at 30 °C and increasing concentrations of LbHsp90. After the binding equilibrium, the samples were excited at 495 nm, and both the parallel and perpendicularly polarized emission components were collected using a long-pass (> 520 nm) filter in a K2 Fluorometer (ISS Inc., Champaign, IL, USA). The fraction of bound Lbp23A or Lbp23B (α) was calculated (36):

$$\alpha = \frac{r_{obs} - r_i}{r_f - r_i} \quad (7)$$

where r_{obs} is the observed anisotropy at each LbHsp90 concentration, and r_i and r_f are the lower and upper asymptotic limits, respectively, for the anisotropy values obtained by curve fitting. K_D values were obtained by fitting the data to a dose–response curve with a variable slope (available in GRAPHPAD PRISM, version 5; GraphPad Software Inc., San Diego, CA, USA) as:

$$y = r_i + \frac{(r_f - r_i)}{\left(1 + e^{((\log K_D - \log[LbHsp90]) * Hillslope)}\right)} \quad (8)$$

Acknowledgements

J. C. Borges thanks the FAPESP (Fundação de Amparo à Pesquisa do Estado de São Paulo) for providing financial support (grants #2007/05001-4, #2011/23110-0, #2012/50161-8) and the CNPq (Conselho Nacional de Pesquisa e Desenvolvimento) for a Research Fellowship grant. We thank the Spectroscopy and Calorimetry Laboratory at Brazilian Biosciences National Laboratory (LNBio/CNPEM-ABTLuS, Campinas, Brazil) for making the AUC and Fluorescence Anisotropy devices available. We also thank the Brazilian Synchrotron Light Laboratory (LNLS/CNPEM-ABTLuS, Campinas, Brazil) for the use of the SAXS beamline. The authors are indebted to the Brazilian financial support agencies CNPq, FAPESP and CAPES (Coordenação de Aperfeiçoamento de Pessoal de Nível Superior) for fellowships.

Author contributions

FAHB, LRSB, SMFM and JCB planned the experiments. FAHB, GSA, TVS, KPS, SMFM and JCB performed the experiments. FAHB, GSA, TVS, LRSB, JCB analyzed the data. FAHB, TVS, JCB organized and conducted the study. FAHB, TVS, JCB prepared the manuscript.

References

1 Borges JC & Ramos CH (2005) Protein folding assisted by chaperones. *Protein Pept Lett* **12**, 257–261.
2 Krukenberg KA, Street TO, Lavery LA & Agard DA (2011) Conformational dynamics of the molecular chaperone Hsp90. *Q Rev Biophys* **44**, 229–255.
3 Li J, Soroka J & Buchner J (2012) The Hsp90 chaperone machinery: conformational dynamics and regulation by co-chaperones. *Biochim Biophys Acta* **1823**, 624–635.
4 Seraphim TV, Ramos CHI & Borges JC (2014) The interaction networks of Hsp70 and Hsp90 in the Plasmodium and Leishmania parasites. In The Molecular Chaperones Interaction Networks in Protein Folding and Degradation (Houry W, ed), pp. 445–481. Springer, New York.
5 Johnson JL & Toft DO (1994) A novel chaperone complex for steroid receptors involving heat shock proteins, immunophilins, and p23. *J Biol Chem* **269**, 24989–24993.
6 Johnson JL, Beito TG, Krco CJ & Toft DO (1994) Characterization of a novel 23-kilodalton protein of unactive progesterone receptor complexes. *Mol Cell Biol* **14**, 1956–1963.
7 Young JC & Hartl FU (2000) Polypeptide release by Hsp90 involves ATP hydrolysis and is enhanced by the co-chaperone p23. *EMBO J* **19**, 5930–5940.
8 Weikl T, Abelmann K & Buchner J (1999) An unstructured C-terminal region of the Hsp90 co-chaperone p23 is important for its chaperone function. *J Mol Biol* **293**, 685–691.
9 Weaver AJ, Sullivan WP, Felts SJ, Owen BA & Toft DO (2000) Crystal structure and activity of human p23, a heat shock protein 90 co-chaperone. *J Biol Chem* **275**, 23045–23052.
10 Forafonov F, Toogun OA, Grad I, Suslova E, Freeman BC & Picard D (2008) p23/Sba1p protects against Hsp90 inhibitors independently of its intrinsic chaperone activity. *Mol Cell Biol* **28**, 3446–3456.
11 Martinez-Yamout MA, Venkitakrishnan RP, Preece NE, Kroon G, Wright PE & Dyson HJ (2006) Localization of sites of interaction between p23 and Hsp90 in solution. *J Biol Chem* **281**, 14457–14464.
12 Panaretou B, Siligardi G, Meyer P, Maloney A, Sullivan JK, Singh S, Millson SH, Clarke PA, Naaby-Hansen S, Stein R *et al.* (2002) Activation of the ATPase activity of hsp90 by the stress-regulated cochaperone aha1. *Mol Cell* **10**, 1307–1318.

13 Richter K, Walter S & Buchner J (2004) The Co-chaperone Sba1 connects the ATPase reaction of Hsp90 to the progression of the chaperone cycle. *J Mol Biol* **342**, 1403–1413.
14 Ali MM, Roe SM, Vaughan CK, Meyer P, Panaretou B, Piper PW, Prodromou C & Pearl LH (2006) Crystal structure of an Hsp90-nucleotide-p23/Sba1 closed chaperone complex. *Nature* **440**, 1013–1017.
15 McLaughlin SH, Sobott F, Yao ZP, Zhang W, Nielsen PR, Grossmann JG, Laue ED, Robinson CV & Jackson SE (2006) The co-chaperone p23 arrests the Hsp90 ATPase cycle to trap client proteins. *J Mol Biol* **356**, 746–758.
16 Chadli A, Bouhouche I, Sullivan W, Stensgard B, McMahon N, Catelli MG & Toft DO (2000) Dimerization and N-terminal domain proximity underlie the function of the molecular chaperone heat shock protein 90. *Proc Natl Acad Sci USA* **97**, 12524–12529.
17 Karagöz GE, Duarte AM, Ippel H, Uetrecht C, Sinnige T, van Rosmalen M, Hausmann J, Heck AJ, Boelens R & Rüdiger SG (2011) N-terminal domain of human Hsp90 triggers binding to the cochaperone p23. *Proc Natl Acad Sci USA* **108**, 580–585.
18 Stebbins CE, Russo AA, Schneider C, Rosen N, Hartl FU & Pavletich NP (1997) Crystal structure of an Hsp90-geldanamycin complex: targeting of a protein chaperone by an antitumor agent. *Cell* **89**, 239–250.
19 Höhfeld J, Cyr DM & Patterson C (2001) From the cradle to the grave: molecular chaperones that may choose between folding and degradation. *EMBO Rep* **2**, 885–890.
20 Bose S, Weikl T, Bügl H & Buchner J (1996) Chaperone function of Hsp90-associated proteins. *Science* **274**, 1715–1717.
21 Freeman BC, Toft DO & Morimoto RI (1996) Molecular chaperone machines: chaperone activities of the cyclophilin Cyp-40 and the steroid aporeceptor-associated protein p23. *Science* **274**, 1718–1720.
22 Felts SJ & Toft DO (2003) p23, a simple protein with complex activities. *Cell Stress Chaperones* **8**, 108–113.
23 WHO (2007) World Heald Organisation: Control of leishmaniasis. Report by the Secretariat.
24 Gonzalez U, Pinart M, Rengifo-Pardo M, Macaya A, Alvar J & Tweed J (2009) Interventions for American cutaneous and mucocutaneous leishmaniasis Cochrane Database of Systematic Reviews Issue 2. CD004834.
25 Croft SL & Olliaro P (2011) Leishmaniasis chemotherapy–challenges and opportunities. *Clin Microbiol Infect* **17**, 1478–1483.
26 Shonhai A (2010) Plasmodial heat shock proteins: targets for chemotherapy. *FEMS Immunol Med Microbiol* **58**, 61–74.
27 Shonhai A, Maier AG, Przyborski JM & Blatch GL (2011) Intracellular protozoan parasites of humans: the role of molecular chaperones in development and pathogenesis. *Protein Pept Lett* **18**, 143–157.
28 Pallavi R, Roy N, Nageshan RK, Talukdar P, Pavithra SR, Reddy R, Venketesh S, Kumar R, Gupta AK, Singh RK *et al.* (2010) Heat shock protein 90 as a drug target against protozoan infections: biochemical characterization of HSP90 from *Plasmodium falciparum* and *Trypanosoma evansi* and evaluation of its inhibitor as a candidate drug. *J Biol Chem* **285**, 37964–37975.
29 Morales MA, Watanabe R, Dacher M, Chafey P, Osorio y Fortéa J, Scott DA, Beverley SM, Ommen G, Clos J, Hem S *et al.* (2010) Phosphoproteome dynamics reveal heat-shock protein complexes specific to the *Leishmania donovani* infectious stage. *Proc Natl Acad Sci USA* **107**, 8381–8386.
30 Khan MY, Villanueva G & Newman SA (1989) On the origin of the positive band in the far-ultraviolet circular dichroic spectrum of fibronectin. *J Biol Chem* **264**, 2139–2142.
31 Royer CA (2006) Probing protein folding and conformational transitions with fluorescence. *Chem Rev* **106**, 1769–1784.
32 Silva JC, Borges JC, Cyr DM, Ramos CH & Torriani IL (2011) Central domain deletions affect the SAXS solution structure and function of yeast Hsp40 proteins Sis1 and Ydj1. *BMC Struct Biol* **11**, 40.
33 Liarte DB & Murta SM (2010) Selection and phenotype characterization of potassium antimony tartrate-resistant populations of four New World Leishmania species. *Parasitol Res* **107**, 205–212.
34 Seraphim TV, Alves MM, Silva IM, Gomes FE, Silva KP, Murta SM, Barbosa LR & Borges JC (2013) Low resolution structural studies indicate that the activator of Hsp90 ATPase 1 (Aha1) of *Leishmania braziliensis* has an elongated shape which allows its interaction with both N- and M-domains of Hsp90. *PLoS One* **8**, e66822.
35 Silva KP, Seraphim TV & Borges JC (2013) Structural and functional studies of *Leishmania braziliensis* Hsp90. *Biochim Biophys Acta* **1834**, 351–361.
36 Siligardi G, Hu B, Panaretou B, Piper PW, Pearl LH & Prodromou C (2004) Co-chaperone regulation of conformational switching in the Hsp90 ATPase cycle. *J Biol Chem* **279**, 51989–51998.
37 Vira S, Mekhedov E, Humphrey G & Blank PS (2010) Fluorescent-labeled antibodies: balancing functionality and degree of labeling. *Anal Biochem* **402**, 146–150.
38 Peacock CS, Seeger K, Harris D, Murphy L, Ruiz JC, Quail MA, Peters N, Adlem E, Tivey A, Aslett M *et al.* (2007) Comparative genomic analysis of three Leishmania species that cause diverse human disease. *Nat Genet* **39**, 839–847.
39 Seraphim TV, Gava LM, Mokry DZ, Cagliari TC, Barbosa LRS, Ramos CHI & Borges JC (2014) The C-terminal region of the human p23 chaperone modulates

its structure and function. *Arch Biochem Biophys*. doi:10.1016/j.abb.2014.10.015.
40 Echtenkamp FJ, Zelin E, Oxelmark E, Woo JI, Andrews BJ, Garabedian M & Freeman BC (2011) Global functional map of the p23 molecular chaperone reveals an extensive cellular network. *Mol Cell* **43**, 229–241.
41 Matrangolo FS, Liarte DB, Andrade LC, de Melo MF, Andrade JM, Ferreira RF, Santiago AS, Pirovani CP, Silva-Pereira RA & Murta SM (2013) Comparative proteomic analysis of antimony-resistant and -susceptible *Leishmania braziliensis* and *Leishmania infantum* chagasi lines. *Mol Biochem Parasitol* **190**, 63–75.
42 Wiser MF (2003) A Plasmodium homologue of cochaperone p23 and its differential expression during the replicative cycle of the malaria parasite. *Parasitol Res* **90**, 166–170.
43 Kobayashi T, Nakatani Y, Tanioka T, Tsujimoto M, Nakajo S, Nakaya K, Murakami M & Kudo I (2004) Regulation of cytosolic prostaglandin E synthase by phosphorylation. *Biochem J* **381**, 59–69.
44 Larkin MA, Blackshields G, Brown NP, Chenna R, McGettigan PA, McWilliam H, Valentin F, Wallace IM, Wilm A, Lopez R *et al.* (2007) Clustal W and Clustal X version 2.0. *Bioinformatics* **23**, 2947–2948.
45 Schuck P, Perugini MA, Gonzales NR, Howlett GJ & Schubert D (2002) Size-distribution analysis of proteins by analytical ultracentrifugation: strategies and application to model systems. *Biophys J* **82**, 1096–1111.
46 Borges JC & Ramos CH (2011) Analysis of molecular targets of *Mycobacterium tuberculosis* by analytical ultracentrifugation. *Curr Med Chem* **18**, 1276–1285.
47 Konarev PV, Volkov VV, Sokolova AV, Koch MHJ & Svergun DI (2003) PRIMUS: a Windows PC-based system for small-angle scattering data analysis. *J App Crystallogr* **36**, 1277–1282.
48 Semenyuk AVS & Svergun DI (1991) *GNOM* – a program package for small-angle scattering data processing. *J Appl Cryst* **24**, 537–540.
49 Svergun DI (1999) Restoring low resolution structure of biological macromolecules from solution scattering using simulated annealing. *Biophys J* **76**, 2879–2886.
50 Volkov VV & Svergun DI (2003) Uniqueness of ab initio shape determination in small-angle scattering. *J Appl Cryst* **36**, 860–864.
51 Ortega A, Amorós D & García de la Torre J (2011) Prediction of hydrodynamic and other solution properties of rigid proteins from atomic- and residue-level models. *Biophys J* **101**, 892–898.
52 Vistica J, Dam J, Balbo A, Yikilmaz E, Mariuzza RA, Rouault TA & Schuck P (2004) Sedimentation equilibrium analysis of protein interactions with global implicit mass conservation constraints and systematic noise decomposition. *Anal Biochem* **326**, 234–256.
53 Johnson ML, Correia JJ, Yphantis DA & Halvorson HR (1981) Analysis of data from the analytical ultracentrifuge by nonlinear least-squares techniques. *Biophys J* **36**, 575–588.